JOURNAL OF MATERIALS SCIENCE 31 (1996) 6477–6483

High-temperature deformation and fracture processes in sintered reaction-bonded silicon nitride

HUA-TAY LIN, J. O. KIGGANS Jr, T. N. TIEGS
Metals and Ceramics Division, Oak Ridge National Laboratory, Oak Ridge, TN 37831, USA

Studies of the high-temperature deformation behaviour of sintered reaction-bonded silicon nitride (SRBSN) materials were conducted at 1200 °C in air under selected stress levels, which were applied at a single stress or as a sequence of stepwise increasing stresses. The objective was to evaluate the effects of the fabrication methods (conventional versus microwave heating process), microstructure, and precursor silicon powder purity on the deformation and fracture processes during creep loading of SRBSN materials containing a mixture of 3 wt % Al_2O_3 and 9 wt % Y_2O_3 sintering additives. Results indicated that all of the SRBSN materials exhibited a threshold stress above which the dominant process underwent transition from creep to extensive creep-assisted crack growth (CACG) from existing pores. In addition, the microwave SRBSN materials exhibited a better resistance (higher threshold stress) to CACG process, compared with those fabricated by conventional heating with the same metallurgical grade of silicon powder. The higher threshold stress observed in microwave SRBSN is mainly associated with the increased number density of elongated grains and the related higher fracture toughness. However, the minimum creep rates and stress exponents obtained in the creep regime were independent of the heating method. The microwave SRBSN material fabricated with lower purity silicon also exhibited a higher threshold stress for multiple crack formation and growth as compared with that processed with higher purity silicon. Conversely, the creep rate of microwave SRBSN materials was decreased by decreasing the impurity level (i.e. iron) in silicon powder.

1. Introduction

Silicon nitride-based materials with elongated grain structure have been considered as one of the most promising candidates for high-temperature structural applications due to their superior thermomechanical properties, such as strength, fracture toughness, and fatigue and creep resistance [1, 2]. However, a major concern in Si_3N_4 materials is to optimize properties but at a much reduced cost. Cost reduction, therefore, has been recognized as a major factor for the successful introduction of advanced ceramics, especially Si_3N_4, into the marketplace [3–5].

Sintered reaction-bonded Si_3N_4 materials are attractive alternatives to the materials made from the more expensive high-purity Si_3N_4 powder [6–8]. The advantages are derived from the facts that (1) silicon powder is much more economical as compared with high-purity Si_3N_4 powder, and (2) SRBSN exhibits less shrinkage than the compacts fabricated with Si_3N_4 powders, providing greater dimensional tolerance and near net shape. Traditionally, the fabrication of SRBSN materials is carried out via a two-step process in a resistance-heated furnace. Recently, microwave heating has been introduced as an alternative process for silicon nitride fabrication [9–14]. In these studies, improved densification during sintering, accelerated nitridation of silicon, and one-step processing of SRBSN have been reported. As a result, microwave heating may provide an economical process route for the fabrication of Si_3N_4 ceramic components.

Several creep studies on RBSN materials fabricated by a two-step conventional heating process have been reported [15–21]. The RBSN materials investigated in those previous cases did not contain oxide densification additives, and the volume fraction of pores was relatively high (~15 %–30 %). The creep rate-controlling process in these RBSN materials was, in general, attributed to a viscous flow (i.e. silicate) of grain-boundary phase which formed due to the internal oxidation of Si_3N_4 grains via open pores and channels during creep at elevated temperatures. As a result, the creep rates of these RBSN materials in an oxidizing environment were found to increase with increases in pore volume fraction and size and impurity content [15–17].

In the present study, the SRBSN materials were fabricated with the addition of 12 wt % oxide densification additives (Al_2O_3 plus Y_2O_3). Thus, the SRBSN investigated contained a relatively large amount of

0022–2461

secondary glassy phase but had much higher final sintered densities (~97%) as compared with the RBSN materials mentioned above. The deformation and fracture processes during creep loading at 1200 °C of microwave SRBSN (MWSRBSN) were compared with the SRBSN fabricated by the conventional heating process (CSRBSN). The effect of the silicon powder purity on the creep rate was also evaluated. This study is part of a larger effort to develop more cost-effective approaches to fabricate Si_3N_4 ceramics and to assess their application limit as high-temperature structural materials [22].

2. Experimental procedure

The starting materials for the SRBSN consisted of appropriate amounts of silicon (metallurgical grade, 3.4 μm mean particle size, < 0.5 wt % impurities:- 0.29% Fe, 0.080% Al, and 0.007% Ca; Elkem Metals Co., Buffalo, NY), α-Si_3N_4 (Stark grade LC-10N, Berlin, Germany), Al_2O_3 (grade RC-HP DBM, Reynolds, Malakoff, TX), and Y_2O_3 (grade 5600, > 99.99%, Molycorp, White Plains, NY), with the final composition after nitriding and sintering to be Si_3N_4–9 wt % Y_2O_3–3 wt % Al_2O_3. A high-purity grade silicon powder (grade Si-HQ, 4.2 μm mean particle size, < 0.05 wt % impurities: 0.038% Fe, 0.08% Al, and 0.015% Ca; Elkem Metals Co., Buffalo, NY) was also employed to evaluate the effect of silicon powder purity on the creep rate. Details of the powder processing of these types of materials have been reported previously [9–12].

All of the SRBSN samples were pre-sintered in argon at 1200 °C for 1 h to obtain densities of 58%–62% theoretical density. All microwave processing was conducted in a 500 l cylindrical microwave cavity operating at 2.45 GHz. The samples were packed in Si_3N_4 powder containing 4 wt % Y_2O_3 and 4 wt % SiC, inside a 15 cm × 15 cm × 12.5 cm alumina fibreboard box. Dense BN heat distributors were used to minimize local hot spots in the samples. Nitridation was performed with N_2–4% H_2–5% He at ~0.1 MPa with additional nitrogen added as the reaction proceeded. After nitridation, the materials were heated to the sintering temperature and maintained for the appropriate time. The MWSRBSN samples were sintered at 1800 °C for 90 min. An entire heating cycle to 1800 °C required approximately 27 h. Further details on the microwave processing can be found in earlier studies [9–12]. The processing of the CSRBSN samples was carried out in resistance-heated graphite furnaces in a two-step process, consisting of a nitridation cycle in one furnace followed by a high-temperature sintering step at 1800 °C for 90 min in a different furnace. The employed nitridation gas and packing powder for CSRBSN materials were the same as those used for MWSRBSN materials. Densities of both types of SRBSN billets were determined by the Archimedes method.

Bend bars (3 mm × 4 mm × > 50 mm) for high-temperature study were prepared using diamond cutting and abrasive grinding wheels. The tensile surfaces of the specimens were machined by surface grinding in a direction parallel to the length of the bars with a 220 grit diamond resinoid-bonded wheel followed by a mechanical polishing through a 0.3 μm diamond paste to obtain a mirror surface finish. The tensile surface edges were bevelled with a 6 μm diamond polishing lap.

The flexural creep tests were conducted at 1200 °C at selected applied stress levels in air. The specimens were loaded in a four-point bending fixture of sintered α-SiC (Carborundum Co., Niagara Falls, NY) with inner and outer spans of 19 and 38 mm, respectively. The stress was directly applied through a sintered α-SiC pushrod using a dead-weight loading system. The test specimens were held at test temperatures for at least 30 min under a stress of ~30 MPa to allow the apparatus to reach a thermal equilibrium condition before raising the stress to the desired level. The stress dependence of the creep rates was obtained by applying a single stress until specimen failure or by stepwise increases in the applied stress for a fixed period of time (~180–200 h) at each stress level. The midspan deflection of the tensile surface of bend bars, with respect to the points on the tensile surface aligned with the inner loading points, was continuously monitored by a high-temperature three-probe extensometer (Applied Test System, Inc., Saxonburg, PA). The creep rate versus time relationship was monitored using the displacement–time data to ensure that a steady state creep rate (or minimum creep rate) had been achieved. The applied stress and resultant creep strain were calculated from the load and displacement data using the procedures described by Hollenberg *et al.* [23].

The microstructures of the as-sintered materials were characterized by both the optical and scanning electron microscopy (SEM). Following creep testing, the specimens were also examined using optical and SEM to characterize the deformation and fracture processes that were a consequence of creep loading and the accumulated creep damage in terms of applied stress level, microstructure, and composition.

3. Results and discussion

3.1. As-sintered microstructure

Fig. 1 shows the typical microstructures of SRBSN materials fabricated by microwave (designated MWSRBSN-HiFe) and conventional (designated CSRBSN-HiFe) heating processes using metallurgical grade (high iron content) silicon powder (< 0.3 wt % Fe impurities, designated HiFe). The microstructure of SRBSN fabricated with high-purity grade silicon powder (< 0.04 wt % Fe impurities, designated LoFe) by microwave processing (designated MWSRBSN-LoFe) is also included for comparison. The polished specimen surfaces were etched in a plasma etching unit (SPI Supplies, West Chester, PA) for ~90 s using a 95% CF_4–5% O_2 gas mixture. SEM observations showed that the secondary amorphous phase formed a continuous network surrounding the β-Si_3N_4 grains. In addition, all of the SRBSN materials exhibited pores ranging in size from 1–15 μm (Fig. 2), which were present after the final sintering stage. The size

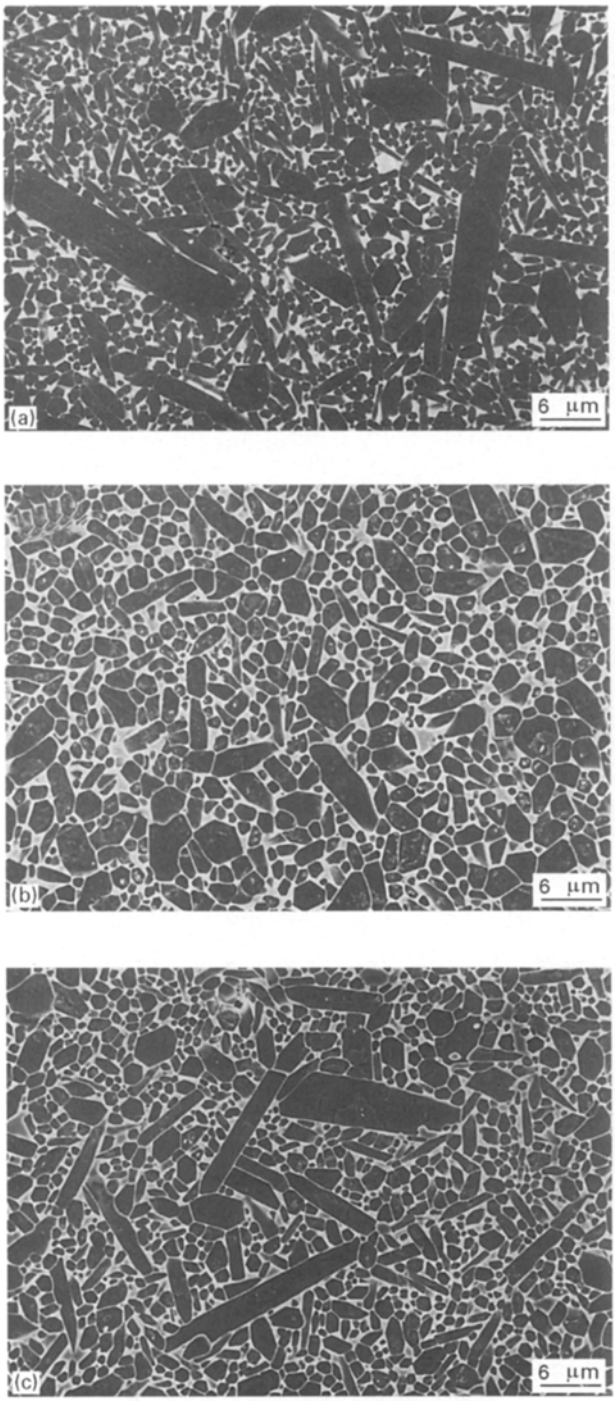

Figure 1 Scanning electron micrographs showing the general microstructure of sintered reaction-bonded silicon nitride (SRBSN). (a) MWSRBSN-HiFe, (b) CSRBSN-HiFe, and (c) MWSRBSN-LoFe.

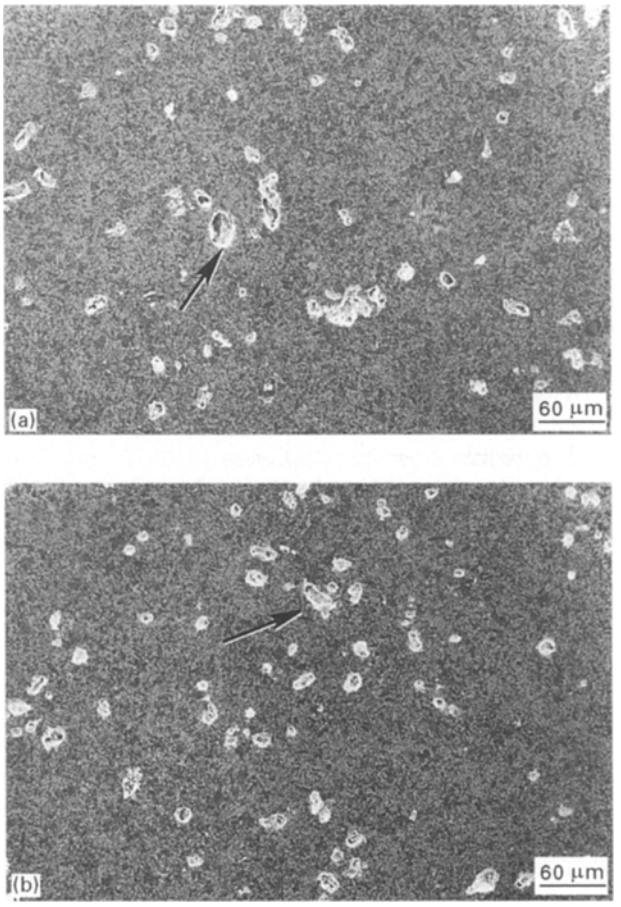

Figure 2 Scanning electron micrographs showing the pore morphology of sintered reaction-bonded silicon nitride (SRBSN). (a) CSRBSN-HiFe, (b) MWSRBSN-HiFe.

and volume number density of pores were not quantitatively analysed, but they were found to be insensitive to sintering method and purity of silicon powder. These samples were dry-pressed from the processed powders and the pore structure was most likely an artefact from this technique. The densities of these SRBSN materials, measured by the Archimedes method, were ~97%–98% theoretical density, independent of processing method and purity of silicon powder. At these sintered densities, the porosity present should consist of closed, isolated pores. Therefore, the effect of internal oxidation via open-pore channels on the creep rates would be minimal. X-ray analyses indicated that all SRBSN materials contained β-Si_3N_4 and a secondary glassy phase.

SEM observations (Fig. 1) showed that the MWSRBSN-HiFe material exhibited a greater fraction of larger elongated grains, with higher aspect ratio (length/diameter), than did the SRBSN processed by conventional heating (CSRBSN-HiFe). The aspect ratio range of the acicular β-Si_3N_4 grains in the CSRBSN-HiFe was ~1–4, while the ratio range for the MWSRBSN-HiFe was ~1–8. The difference in elongated grain microstructure between MWSRBSN-HiFe and CSRBSN-HiFe was largely attributed to the enhanced microwave coupling effect with the liquid phase, resulting in more acicular grain growth in MWSRBSN- HiFe [24, 25]. In addition, the SRBSN material made with the higher purity silicon powder (MWSRBSN-LoFe) exhibited an aspect ratio range (~1–7) similar to that fabricated with high iron content silicon powder (MWSRBSN-HiFe). However, the number density of larger β-Si_3N_4 grains with a high aspect ratio (~8) in the MWSRBSN-LoFe was about two-times less than those in the MWSRBSN-HiFe (Fig. 1). Previous studies by Tiegs *et al.* [11] reported that the samples (MWSRBSN-HiFe) fabricated with lower purity silicon powder contained more α-phase (~70%) as compared with that (MWSRBSN-LoFe) processed with the higher purity silicon powder ($< 50\%$) after nitridation in a microwave furnace. The presence of iron impurity in silicon powder is

known catalytically to accelerate the nitridation rate due to the formation of an $FeSi_2$ liquid phase at a eutectic temperature of 1208 °C [26, 27]. The presence of $FeSi_2$ alloy, as the liquid transport medium, enhances the formation of the α-phase particles via the vapour–liquid–solid mechanism [26]. Because the growth of the β-Si_3N_4 grains occurred by solution of the initial α-particles present and the reprecipitation of Si_3N_4 on the pre-existing β-particles, the higher initial α-phase content would result in more elongated grain growth during the α to β transformation and improved mechanical properties [28].

As a result of these highly developed elongated-grain microstructures, the MWSRBSN-HiFe exhibited a higher fracture toughness (8.7 MPa $m^{1/2}$) as compared with CSRBSN-HiFe (5.7 MPa $m^{1/2}$) or MWSRBSN-LoFe (7.0 MPa $m^{1/2}$). The fracture toughness in the present study was measured by a controlled-flaw and fracture method with the 294 N Vickers indents and crack length of ~340–480 μm [29]. Previous studies have demonstrated that the ceramic materials with higher toughness and *R*-curve behaviour exhibit higher tolerance to flaws introduced during processing or service [30, 31]. The study conducted by Tajima *et al.* [31] showed that the low-toughness materials exhibited a substantial decrease in strength with a decrease in grit of the diamond grinding wheel, whereas the highest toughness material showed almost no degradation in strength, regardless of machining conditions. Therefore, it is anticipated that the MWSRBSN-HiFe should exhibit higher resistance to process- or service-induced flaws and damage than either the CSRBSN-HiFe or MWSRBSN-LoFe materials. Furthermore, the MWSRBSN-HiFe also exhibited the highest room-temperature flexural strength (744 ± 50 MPa) with respect to MWSRBSN-LoFe (687 ± 57 MPa) and CSRBSN-HiFe (600 ± 66 MPa). Because the pore volume fraction and morphology in all these SRBSN materials are similar, the difference in fracture strengths may result from variations in the fraction of larger elongated grains present.

3.2. High-temperature deformation behaviour

Fig. 3 illustrates the typical creep strain versus time curves for MWSRBSN-HiFe specimens, which were under a single applied stress of 175 or 200 MPa at 1200 °C in air. Generally, the test specimens with short creep lives always failed in the primary creep regime (shown in Fig. 1b) and those which could sustain the applied load up to 250 h without specimen failure exhibited a primary stage followed by a long apparent secondary stage (Fig. 1a). Therefore, the creep data obtained from single-stress tests for all the SRBSN materials include the creep rates obtained in primary stage, $\dot{\varepsilon}_{primary}$, and in the apparent minimum creep stage, $\dot{\varepsilon}_{min}$, as will be depicted below.

Fig. 4 summarizes the creep results at 1200 °C and at stress levels from 75–250 MPa in air for SRBSN materials fabricated by microwave (MWSRBSN-HiFe) and conventional (CSRBSN-HiFe) heating processes. These two SRBSN materials were fabricated with the same metallurgical grade (high iron content) of silicon powder. The creep data were obtained from single-stress or multiple-stress tests. Results from the single-stress tests indicated that a threshold stress existed above which both MWSRBSN-HiFe and CSRBSN-HiFe exhibited higher creep rates and

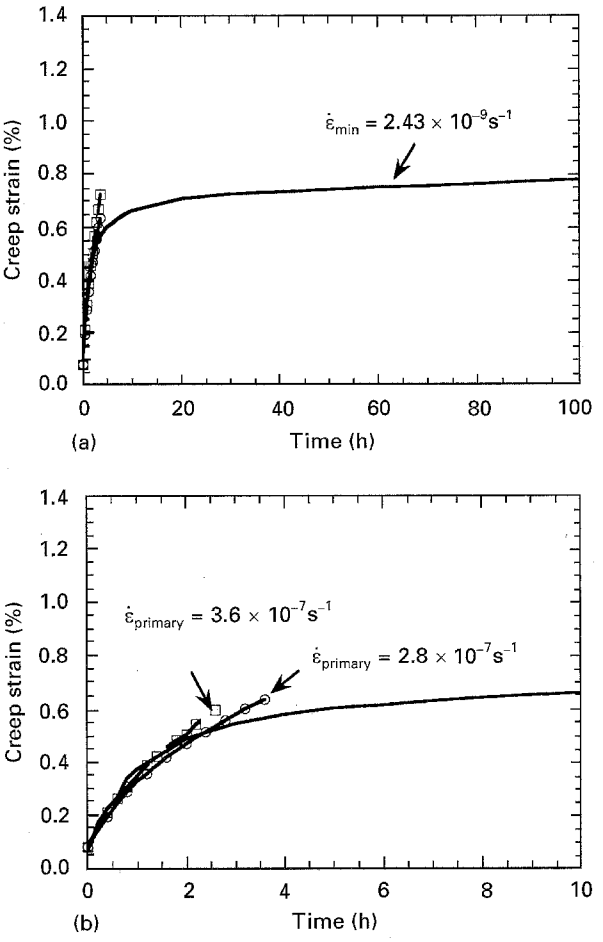

Figure 3 Creep strain versus time curves for MWSRBSN-HiFe tested at 1200 °C under an applied stress of 175 or 200 MPa. (a) (–○–) 175 MPa, t_f = 3.6 h; (–□–) 200 MPa, t_f = 3 h, (—) 175 MPa for 210 h. (b) (–○–) 175 MPa, t_f = 3.6 h; (–□–) 200 MPa, t_f = 2.5 h; (—) 175 MPa for 210 h.

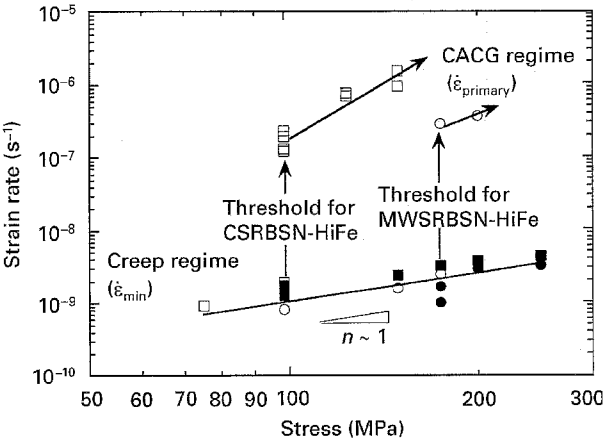

Figure 4 Strain rate versus applied stress curves for (●, ○) MWSRBSN-HiFe and (■, □) CSRBSN-HiFe materials. Note that the MWSRBSN-HiFe exhibited a higher threshold stress for creep-assisted crack growth than the CSRBSN-HiFe. (●, ■) Step σ (○, □) single σ.

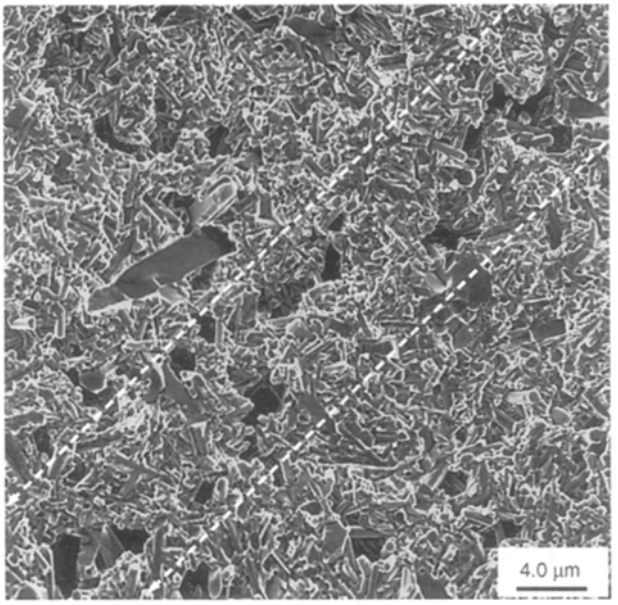

Figure 5 Scanning electron micrograph of the fracture surface in the tensile surface region of MWSRBSN-HiFe tested at 1200 °C and at 175 MPa with creep life of 3.6 h. Extensive crack formation and growth, formed as a band of cavities linkage, was observed in the specimens failed in the primary creep stage.

shorter creep lives ($\sim$0.2–3 h) accompanied by higher stress exponents. In the regime below the threshold stress, both SRBSN materials exhibited similar low creep rates ($\sim 10^{-9}\,s^{-1}$) and low stress exponents ($n \sim 1$), indicative of a creep-dominant process (creep regime). The threshold stress was $\sim$175 MPa for MWSRBSN-HiFe and $\sim$100 MPa for CSRBSN-HiFe. The transition to high creep rates and short creep lives was found to be associated with the occurrence of extensive multiple crack formation and growth (Fig. 5).

Fig. 5 shows the fracture surface of MWSRBSN-HiFe specimen tested at 175 MPa and failed in the primary stage with creep life of 3.6 h. The fracture surface was created at room temperature in a direction perpendicular to the original high-temperature fracture surface and parallel to the tensile stress orientation. The fracture surface revealed features of extensive multiple crack formation and growth, which were initiated at existing pores. Similar features were also observed in the CSRBSN-HiFe materials. The observations suggested that at stresses above the threshold level, the cracks initiated and grew from the existing pores, which served as the stress concentration sites for crack and creep cavity initiation, and coalesced and rapidly reached a critical size during the primary creep stage, ultimately leading to catastrophic failure with short creep life for both MWSRBSN and CSRBSN materials. The creep deformation processes, such as grain-boundary sliding and the diffusional process via the intergranular amorphous phase, would further assist this multiple crack-growth process. Observations also showed that the size of the damage zone developed in the MWSRBSN-HiFe specimens tested at 175 MPa was at least five times larger than those in the CSRBSN-HiFe specimens tested at 175 MPa (as is evident in Fig. 6). The greater resistance (i.e. higher threshold stress) to the creep-assisted crack growth (CACG) process observed in the MWSRBSN-HiFe material is attributed to its higher fraction of larger elongated grains (Fig. 1) and higher room-temperature fracture toughness as compared with CSRBSN-HiFe material. Furthermore, the larger elongated grains in the MWSRBSN-HiFe material will more effectively bridge the crack developed during creep loading and be able to sustain a larger damage zone prior to fracture with respect to the CSRBSN-HiFe material when tested at the same stress level above the threshold stress.

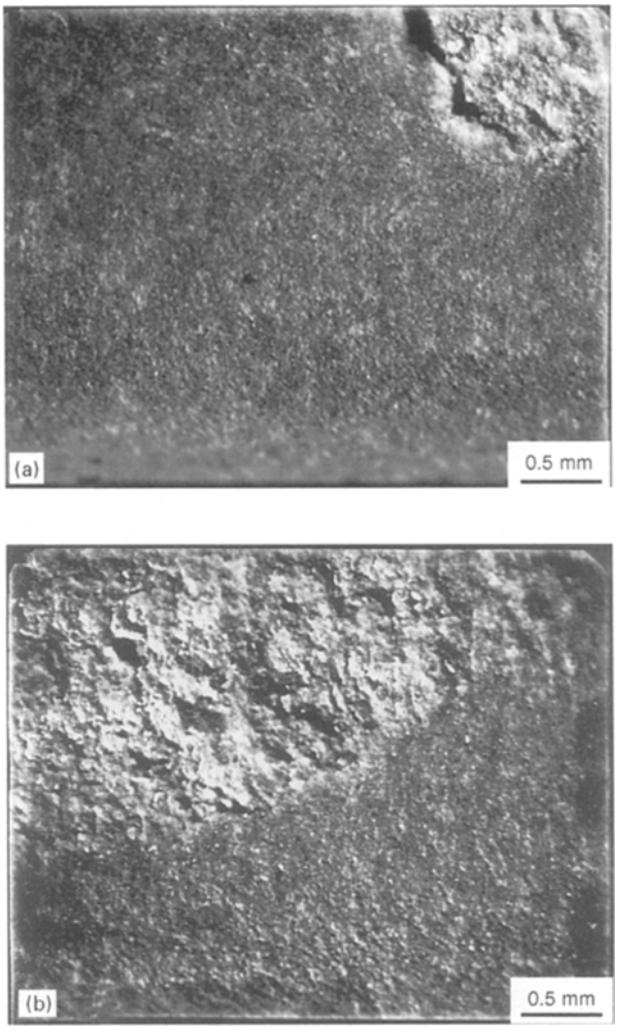

Figure 6 Fracture surface features of (a) CSRBSN and (b) MWSRBSN samples tested at 1200 °C and at 175 MPa with failure occurring in the primary creep stage. Note the damage zone developed in the MWSRBSN is four times larger than that in the CSRBSN.

On the other hand, the creep data obtained under sequential multiple-stress, always starting with stress levels below the threshold stress for CACG process, revealed that both MWSRBSN-HiFe and CSRBSN-HiFe can be subjected to stresses up to 250 MPa for at least 200 h without causing specimen failure. In addition, results from single stress tests below the threshold and multiple stress tests indicated that both SRBSN materials exhibited similar creep rates and stress exponents ($n \sim 1$) under the stress levels employed, independent of fabrication process. Such a low stress exponent ($n \sim 1$) is consistent with either

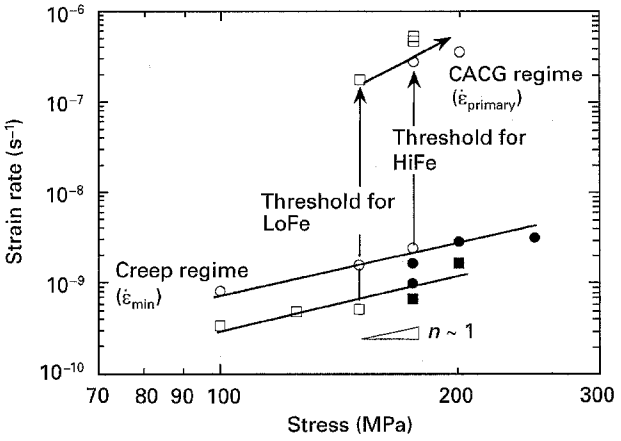

Figure 7 Strain rate versus applied stress curves for MWSRBSN materials fabricated with (●, ○) metallurgical grade (0.3% Fe, HiFe) and (■, □) high-purity grade (0.04% Fe, LoFe) silicon powder. Note that the MWSRBSN-LoFe exhibited a lower threshold stress for creep-assisted crack growth, but better creep resistance as compared with MWSRBSN-HiFe. (●, ■) Step σ, (○, □) single σ.

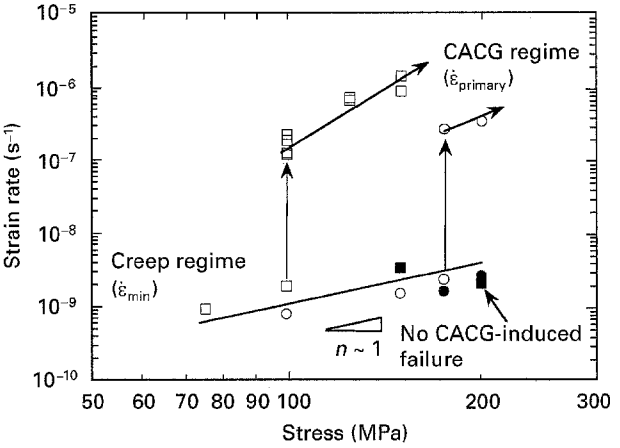

Figure 8 Strain rate versus applied stress curves for (○, ●) MWSRBSN-HiFe and CSRBSN-HiFe materials in the (□) as-sintered or (■) as-annealed condition. The post-annealing at 1200 °C increased the threshold stress for creep-assisted crack growth.

diffusional or viscous creep processes associated with amorphous grain-boundary phase(s) [32–35]. Similar stress exponents ($n < 2$) were also reported for creep studies of RBSN materials without oxide sintering additives [15–18]. In those previous studies, creep was attributed to the viscous flow of the grain-boundary phase (i.e. silicate) formed due to the oxidation of Si_3N_4 grains through the open pore channels. As the sintered density of all the SRBSN investigated in the present study was ~97%, the pores present would be isolated and closed ones. The influence of internal oxidation through open-pore channels on the creep results obtained in the present study will be therefore very limited.

The creep results of MWSRBSN materials fabricated using high (MWSRBSN-HiFe) and low (MWSRBSN-LoFe) iron content silicon powders are summarized in Fig. 7. The relative impurity levels (mainly iron) in MWSRBSN-HiFe and MWSRBSN-LoFe materials are 0.3 and 0.04 wt %, respectively. Results from single-stress tests revealed that MWSRBSN-LoFe material exhibited a relatively low threshold stress (~150 MPa) for the transition to a CACG process with respect to that obtained for the MWSRBSN-HiFe material (~175 MPa). This is consistent with the lower fraction of larger elongated grains (as seen in Fig. 1) and lower toughness value in the MWSRBSN-LoFe material. On the other hand, data from single stress tests below the threshold, and sequential multiple-stress tests, indicated that the creep resistance of MWSRBSN materials may be improved somewhat by reducing the silicon powder impurity (i.e. iron) levels. For instance, the MWRBSN-LoFe material exhibited creep rates that were slightly (~ three-fold) lower than the MWRBSN-HiFe material under the same applied stress levels at 1200 °C. Iron remains in the intergranular amorphous phase where it reduces the viscosity and softening temperature, thus enhancing the creep rates. The stress exponent was approximately 1 for both MWSRBSN materials, indicative of diffusional or viscous flow creep process.

As seen from the single-stress tests, all the SRBSN materials exhibited a threshold stress above which the materials fractured by the occurrence of extensive multiple crack generation and growth, and below the threshold the deformation in SRBSN was governed by the diffusional or viscous creep processes. Above the threshold level, extensive microcracks formed and grew from existing pores. The growth of these micro cracks would be further assisted by the creep deformation processes via continuous nucleation, growth and coalescence of creep cavities. The rapid development of damage zone within the critical crack-tip process zone by a continuous linkage and growth of micro cracks led to final failure of the materials as the damage accumulation ultimately reached the critical size. The threshold stress for the CACG process to occur was observed to increase with the fraction of larger Si_3N_4 grains with high aspect ratio, consistent with the measured fracture toughness values as discussed in the previous section. The MWSRBSN-HiFe material with the highest fracture toughness exhibited a better resistance (a higher threshold stress) to the CACG process as compared with either the CSRBSN-HiFe or MWSRBSN-LoFe materials.

On the other hand, for sequential multiple-stress tests that began at a stress below the threshold for CACG process, the applied stress could be sequentially increased up to 250 MPa without any specimen failure. Therefore, a heat treatment at 1200 °C in air for 100 h was conducted on both MWSRBSN-HiFe and CSRBSN-HiFe materials prior to creep tests to evaluate the effect of oxidation on the CACG susceptibility. Creep results at 1200 °C for both SRBSN materials showed that an initial single stress up to 200 MPa can be applied on the annealed specimens for up to 200 h without any specimen failure (Fig. 8). Additional experiments showed that the creep rates and stress exponent of annealed specimens under a single-stress test were similar to those obtained from sequential multiple-stress tests without heat treatment in air. Results suggested that the heat treatment at 1200 °C in air prior to creep testing could seal the tensile surface and blunt the microstructural defects through the SiO_2 formation, resulting in an increased threshold stress ($\geqslant$ 200 MPa). Similar observations of enhancement in creep properties were also reported previously

for RBSN materials annealed at 1400 °C in air [16]. Further detailed studies are under way to explore the effect of various heat-treatment processes on the creep response of SRBSN materials.

4. Conclusion

Studies of high-temperature deformation and fracture behaviour in SRBSN materials fabricated by microwave and conventional heating processes indicated that the MWSRBSN materials exhibited a better resistance to the creep-assisted crack growth process, which initiated at the existing microstructural defects (i.e. pores). The enhancement in resistance to the creep-assisted crack-growth process was largely associated with the increased elongated grain growth by microwave heating, consistent with the fracture toughness results. On the other hand, in the creep regime both SRBSN materials exhibited similar creep behaviour, low creep rate and stress exponent ($n \sim 1$), independent of the heating process. The stress exponent of 1 was attributed to diffusional or viscous creep processes. Creep results also indicated that the microwave SRBSN containing lower purity silicon powder revealed a higher threshold stress for creep-assisted crack growth as compared with that processed with higher purity powder due to an increased fraction of large elongated grains. But, the creep rate of microwave SRBSN was reduced by increasing the silicon powder purity (decreasing iron impurity). A heat treatment at 1200 °C in air prior to creep testing resulted in the sealing of the tensile surface and blunting of pores due to formation of SiO_2, reducing the susceptibility to the creep-assisted crack-growth process.

Acknowledgements

The authors thank Drs K. P. Plucknett, A. A. Wereszczak and P. F. Becher, for reviewing the manuscript. This research was sponsored by the US Department of Energy, Assistant Secretary for Energy Efficiency and Renewable Energy, Office of Transportation Technologies, as part of the Ceramic Technology Project of the Propulsion System Materials Program, under contract DE-AC05-96OR22464 with Lockheed Martin Energy Research, Corp.

References

1. D. W. RICHERSON and P. M. STEPHAN, *Mater. Sci. Forum* **47** (1989) 282.
2. M. MATSUI, in "MRS symposium proceedings," Vol. 287, edited by I.-W. Chen, P. F. Becher, M. Mitomo, G. Petzow and T.-S. Yen, "Silicon Nitride Ceramics Scientific and Technical Advances" (Materials Research Society, Pittsburgh, PA, 1993) pp. 173–88.
3. L. M. SHEPPARD, *Am. Ceram. Soc. Bull.* **70** (1991) 692.
4. T. QUADIR, R. W. RICE, J. C. CHAKRAVERTY, J. A. BREINDEL and C. C. WU, *Ceram. Eng. Sci. Proc.* **12** (1991) 1952.
5. J. M. SCHOENUNG, *Am. Ceram. Soc. Bull.* **71** (1992) 1103.
6. A. J. MOULSON, *J. Mater. Sci.* **14** (1979) 1017.
7. F. L. RILEY (ed), in "Nitrogen Ceramics," (Noordhoff, The Netherlands, 1977) pp. 265–88.
8. J. A. MANGELS and G. J. TENNENHOUSE, *Am. Ceram. Soc. Bull.* **59** (1980) 1216.
9. T. N. TIEGS, J. O. KIGGANS and H. D. KIMREY, in "Microwave Processing of Materials-II," Vol. 189, edited by W. B. Snyder, W. H. Sutton, D. L. Johnson and M. F. Iskander (Materials Research Society, Pittsburgh, PA, 1991) pp. 267–72.
10. T. N. TIEGS, J. O. KIGGANS and K. L. PLOETZ, *Ceram. Eng. Sci. Proc.* **14** (1993) 378.
11. *Idem*, in "Materials Research Society Symposium Proceedings," Vol. 287, edited by I.-W. Chen, P. F. Becher, M. Mitomo, G. Petzow and T.-S. Yen. (Materials Research Society, Pittsburgh, PA, 1993) pp. 283–88.
12. J. O. KIGGANS, T. N. TIEGS, H. D. KIMREY and C. E. HOLCOMBE, in "Ceramic Transactions, Microwaves: Theory and Application in Materials Processing II", edited by D. E. Clark, W. R. Tigna and J. R. Laia Jr. (American Ceramic Society, Westerville, OH, 1993) pp. 269–76.
13. M. L. C. PATTERSON, P. S. APTE, R. M. KIMBER and R. ROY, in "Microwave Processing of Materials-III", Vol. 269, edited by R. L. Beatty, W. H. Sutton and M. F. Iskander (Materials Research Society, Pittsburgh, PA, 1992) pp. 291–300.
14. J. ZHANG, L. CAO and F. XIA, *ibid.*, pp. 329–34.
15. G. GRATHWOHL and F. THÜMMLER, *J. Mater. Sci.* **13** (1978) 1177.
16. F. THÜMMLER and G. GRATHWOHL, in "Progress in Nitrogen Ceramics", edited by F. L. Riley (Martinus Nijhoff, The Netherlands, 1983) pp. 547–55.
17. J. HEINRICH, D. MUNZ and G. ZIEGLER, *Powder Metall. Int.* **14** (3) (1982) 153.
18. S. U. DIN and P. S. NICHOLSON, *J. Am. Ceram. Soc.* **58** (1975) 500.
19. J. M. BIRCH, B. WILSHIRE and D. J. GODFREY, *Proc. Brit. Ceram. Soc.* **26** (1978) 141.
20. F. PORZ, G. GRATHWOHL and F. THÜMMLER, *ibid.* **31** (1981) 157.
21. T. SOMA, M. MATSUI and I. ODA, in "Materials Science Research", Vol. 8, "Deformation of Ceramic Materials II", edited by R. E. Tressler and R. C. Bradt (Plenum Press, New York, 1984) pp. 379–89.
22. D. R. JOHNSON (ed) in Ceramic Technology Project Semi-annual Progress Report for October 1993 through March 1994", ORNL/TM-12778 (Oak Ridge National Laboratory, Oak Ridge, TN, 1994) pp. 1–2.
23. G. W. HOLLENBERG, G. R. TERWILLIGER and R. S. GORDON, *J. Am. Ceram. Soc.* **54** (1971) 196.
24. D. R. CLARKE and W. W. HO, in "Additives and Interfaces in Electronic Ceramics, Advances in Ceramics", Vol. 7, edited by M. F. Yan and A. H. Heuer (American Ceramic Society, Westerville, OH, 1983) pp. 246–52.
25. H. OHNO and Y. KATANO, *Mater. Sci. Forum* **47** (1989) 215.
26. D. R. MESSIER and P. WONG, *J. Am. Ceram. Soc.* **56** (1973) 480.
27. A. de S. JAYATILAKA and J. A. LEAKE, in "Nitrogen Ceramics", edited by F. L. Riley, (Noordhoff International, The Netherlands, 1977) pp. 289–94.
28. F.F. LANGE, *J. Am. Ceram. Soc.* **62** (1979) 428.
29. R. F. COOK and B. R. LAWN, *J. Am. Ceram. Soc.* **66** (1983) C-200.
30. C. W. LI, C. J. GASDASKA, J. GOLDACKER and S-C. LUI, in "Materials Research Society Symposium Proceedings," Vol. 287 (Materials Research Society, Pittsburgh, PA, 1993) pp. 473–80.
31. Y. TAJIMA and K. URASHIMA, in "Tailoring of Mechanical Properties of Si_3N_4 Ceramics," edited by M. J. Hoffmann and G. Petzow (Kluwer Academic, The Netherlands, 1994) pp. 101–9.
32. G. ZIEGLER, *Mater. Sci. Forum* **47** (1989) 162.
33. J. R. DRYDEN, D. KUCEROVKY, D. S. WILKINSON and D. F. WATT, *Acta Metall.* **37** (1989) 2007.
34. R. L. TSAI and R. RAJ, *ibid.* **30** (1982) 1043.
35. F. F. LANGE, in "Deformation of Ceramic Materials", edited by R. C. Bradt and R. E. Tressler (Plenum, New York, 1976) pp. 361–81.

Received 2 October 1995
and accepted 8 May 1996